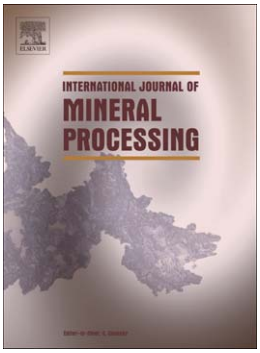

Experimental quantification of turbulence and its applications in the study of multiphase flotation pulps

Weiguo Xie, Jun Meng, Anh V. Nguyen

PII: S0301-7516(16)30146-6
DOI: doi: 10.1016/j.minpro.2016.06.011
Reference: MINPRO 2924

To appear in: *International Journal of Mineral Processing*

Received date: 24 February 2016
Revised date: 24 June 2016
Accepted date: 28 June 2016

Please cite this article as: Xie, Weiguo, Meng, Jun, Nguyen, Anh V., Experimental quantification of turbulence and its applications in the study of multiphase flotation pulps, *International Journal of Mineral Processing* (2016), doi: 10.1016/j.minpro.2016.06.011

Experimental Quantification of Turbulence and its Applications in the study of Multiphase Flotation Pulps

Weiguo Xie[*1], Jun Meng[1], Anh V. Nguyen[2]

[1] Julius Kruttschnitt Mineral Research Centre, 40 Isles Road, Indooroopilly, QLD 4068, Australia

[2] School of Chemical Engineering, The University of Queensland, St Lucia, QLD 4072, Australia

Abstract

Turbulence is common in daily activities, both naturally and industrially. However, it is not well understood on the microscopic level because there is a lack of suitable quantification techniques especially for multi-phase particulate systems such as flotation pulps. In this paper, the different quantification techniques which have been used to characterise turbulence in the literature have been reviewed in terms of their basic principles, system structure, the range of application and limitations. Optical techniques such as Laser Doppler Anemometry and Particle Image Velocimetry can produce accurate measurement results with high spatial and temporal resolution, but their applications are limited to transparent flows. Hot wire probes have high spatial and temporal resolution in turbulence quantification, but they are susceptible to environmental factors. Conductivity probe, Electrical Resistance Tomography (ERT) and Piezoelectric Sensor are techniques that can quantify turbulence in multiphase flows, but their spatial resolutions are limited. Particle Tracking Velocimetry can reveal particle trajectories in multiphase flows; it can also measure velocity fluctuation. Positron Emission Particle Tracking cannot be used to quantify turbulence although it can also be used to determine the Lagrangian trajectory of particles. For turbulence quantification in three phase flows, piezoelectric sensor, ERT and conductivity probe require further development.

Keywords: turbulence, quantification techniques, ERT, piezoelectric sensors, conductivity probe

1. Introduction

The American Nobel Prize Laureate for Physics Richard Feynman once described turbulence as "the most important unsolved problem of classical physics" (Eames & Flor,2011), because a description of the phenomenon from first principles does not exist. British fluid dynamicist, Horace Lamb, at a meeting of the British Association in London in 1932, he stated, "When I die and go to heaven there are two matters on which I hope for enlightenment. One is quantum electrodynamics and the other is the turbulent motion of fluids. About the former I am rather optimistic" (Tabor,1989). It is no doubt that turbulence brings a significant scientific challenge even in today, although it was revealed phenomenologically long time ago.

The complexity of turbulence lies in the irregular motion of fluids in a broad range of different scales. Especially when the system is of three-phase (solid, liquid and gas) such as the pulp phase in flotation cells, the instant local physical quantities (such as velocity, pressure, density, temperature, bubble size distribution, etc.) in the system just display randomly within a quite wide range. Under normal circumstances, turbulence flow in continuum phase can be described by the Navier – Stokes equations. Nonlinearity of the Navier – Stokes equations leads to interactions between fluctuations of differing wavelengths and directions (Wilcox,1998). The large – scale turbulent motion carries most of the energy and is mainly responsible for the enhanced diffusivity and attending stresses. The energy is dissipated from large eddies to smaller eddies till the shortest wavelengths by viscosity.

In a turbulent flow, the instant local physical quantities may be decomposed into a mean part and a fluctuating part, which now called the Reynolds decomposition (Avila *et al.*,2011). Averaging the equations gives the Reynolds-averaged Navier–Stokes (RANS) equations, which govern the mean flow. The root-mean-square value of the fluctuations and the frequency of change of sign of the fluctuations are quantitative measures of turbulence (Streeter,1966). Therefore, the quantification of turbulence has focussed on the fluctuating part of the physical quantities.

In this paper, turbulence theory and applications will be briefly discussed, then followed by the section of turbulence quantification methods and technologies. There are many existing turbulence quantification techniques, such as Laser Doppler Anemometry (LDA), Particle Image Velocimetry (PIV), Constant Temperature Anemometer (CTA), Positron Emission Particle Tracking (PEPT), Piezoelectric Vibration Sensor (PVS) and Electrical Resistance Tomography (ERT). All those

[*]Corresponding author: Dr. Weiguo Xie，Julius Kruttschnitt Mineral Research Centre, University of Queensland, Senior Research Fellow, 40 Isles Road Indooroopilly, QLD 4068, Australia. Phone: +61733465934. Email: w.xie@uq.edu.au

techniques will be reviewed regarding their basic principles, system structure, the range of application and limitations.

2. Turbulence Theory and Applications

2.1 Turbulence Theory

In fluid dynamics, turbulence is flow characterized by recirculation, eddies, and apparent randomness. The main features of turbulence (Mathieu & Scott,2000) are:

- It is a random process in terms of time and space.
- It contains a wide range of different scales.
- It arises at high Reynolds numbers.
- It dissipates energy.

In laminar flow regime, fluid particles move along smooth paths in laminas with one layer gliding smoothly over an adjacent layer, in which the action of viscosity damps out turbulent tendencies (Streeter, 1966). While in turbulent flow regime, it has low momentum diffusion, high momentum convection, and rapid change of pressure and flow velocity in space and time. It is characterised by the Reynolds number (Batchelor,1967; Streeter,1966) which is the ratio of inertial forces to viscous forces in a fluid flow:

$$R_e = \frac{VL}{\nu} \tag{1}$$

where *V* is the mean velocity, *L* is the characteristic length and ν is the kinematic viscosity.

In general, the intensity of turbulence increases as the Reynolds number increases (Streeter, 1966). Reynolds number has been recognised as an indicative quantity for the turbulence in flow through tubes (Batchelor, 1967). When the Reynolds number is low (<2000), the flow tends to be laminar, while a high Reynolds number (>4000) is an indication that the flow is turbulent(Holman,2002). However, there is no theorem relating the dimensionless Reynolds number (Re) to turbulence. In pipe flow, for example, turbulence can first be sustained if the Reynolds number is typically ranging from 1700 to 2300, and occasionally even values more than 3000 are quoted (Avila *et al.*, 2011).

Although the turbulent flow appears random in time and space and is not reproducible in detail, researchers suggested that turbulent flow is governed by the same fundamental equations as laminar flow, the Navier–Stokes equation (Mathieu and Scott, 2000). The basic rationality is to assume the disorder in turbulent flow from the consequence of the equation rather than in a breakdown of the quantitative model.

The Navier–Stokes equation has been well-used as the governing equation for the motion of fluid (Batchelor, 1967):

$$\rho \frac{Du_i}{Dt} = \rho F_i - \frac{\partial p}{\partial x_i} + \frac{\partial}{\partial x_j}\{2\mu(e_{ij} - \frac{1}{3}\Delta\delta_{ij})\} \tag{2}$$

where, ρ is the density of fluid, $\frac{Du_i}{Dt} = \frac{\partial u_i}{\partial t} + u \cdot \nabla u_i$, F_i is conservative body force per unit mass, p is the pressure in the fluid, μ is the viscosity of the fluid, $e_{ij} = \frac{1}{2}(\frac{\partial u_j}{\partial x_i} + \frac{\partial u_j}{\partial x_i})$ is rate-of-strain tensor. $\Delta = \nabla \cdot u$ is the rate of expansion.

The Reynolds-averaged Navier–Stokes equations (or RANS equations) are time-averaged equations based on the Navier–Stokes equation. For incompressible Newtonian fluid, these equations can be written as (Wilcox, 1998):

$$\rho \frac{\partial \overline{u_i}}{\partial t} + \rho \overline{u_j} \frac{\partial \overline{u_i}}{\partial x_j} = \rho F_i - \frac{\partial p}{\partial x_i} + \frac{\partial}{\partial x_j}\{2\mu(e_{ij} - \rho \overline{u_j' u_i'})\} \tag{3}$$

Reynolds' equations for the mean velocity demonstrated the so-called ''closure problem'' in turbulence: if one generates from the Navier-Stokes equations an auxiliary equation for a low-order moment such as the mean value, that equation contains higher-order moments, therefore, at any level there is always one unknown more than the available equations. Thus, even though the Reynolds-averaged Navier-Stokes equations are themselves closed, some additional assumptions are required to close the set of auxiliary equations at any specific level.

Turbulence has a wide range of different scales. There are some of the most useful scales for describing turbulence, such as Kolmogorov length, velocity and time scales, and integral length scale. The velocity correlation is performed to determine the order of the size of the largest spatial scales of turbulence length, L, which characterizes the spatial separation required for significant decorrelation of the velocity fluctuations (Mathieu and Scott, 2000). When this velocity correlation is successively performed, the spatial structure of the velocity field scaled down to the smallest, known as Kolmogorov length scale η (Equation 4), at which it appears smooth (Kolmogorov,1941).

$$\eta = (\nu^3/\epsilon)^{1/4} \tag{4}$$

where ν is kinematic viscosity, ϵ is the dissipation rate.

Turbulence dissipates energy, turbulence kinetic energy, from large eddies to small eddies through cascade process. Dissipation of kinetic energy to heat through the action of molecular viscosity occurs at the scale of the smallest eddies at Kolmogorov length, velocity and time scales (Wilcox, 1998).

2.2 Turbulence Applications in Minerals Processing

Flows that are most commonly seen in practical engineering are turbulent (Wilcox, 1998). The large Reynolds number, which indicates the onset of turbulence, is quite easy to achieve in water or air systems, such as river currents or motion of vehicles. Due to main features of turbulence are of highly efficient on both energy dissipation and mass transfer, turbulence gains wide applications in minerals industries.

In stirred tanks, an intense turbulence produced enables fast micromixing and thus a very high mass transfer rate (Wu *et al.*,2012). The process intensification to enhance turbulence can lead to dramatically increased throughput for large-scale processing reactors, especially for the minerals industry. The flow regions of a stirred tank may be classified into the impeller stream flowing radially towards the wall, the recirculation regions, and the region surrounding the impeller where the circulation loops meet (Rao & Brodkey,1972). The flow region with the highest turbulence is the impeller stream (Cutter,1966; Rao & Brodkey,1972). Rao and Brodkey calculated integral velocity scales from the autocorrelation after subtracting the contribution of the periodic velocities, and velocity microscales and energy dissipation rates mostly from the derivative signals of the fluctuating velocities.

In bubble column, turbulence is induced in the liquid by the movement of the bubbles due to shear produced in the vicinity of the bubbles, in particular due to bubble oscillations and wakes(Sanyal *et al.*,1999; Laín *et al.*,2002). Bubbly flows occur in a variety of industrial processes, such as elaboration of alloys, two-phase heat exchangers, aeration and stirring of reactors, flotation devices, and bubble column reactors. Bubble columns, in which a large number of gas bubbles rise through a liquid, are frequently encountered in the chemical, petrochemical, and biotechnological industries.

Turbulence plays an important role in the flotation process (Fallenius,1987; Schubert,1999; Nguyen & Schulze,2004; Evans *et al.*,2008), including three important effects of turbulence: the first is that it affects the transport of solids (and therefore the suspension of solid fine grains) through its effect on the macro-turbulence properties in the tank; the other two are gas dispersion and particle-bubble collision, attachment and detachment, which are all controlled by micro-turbulence. In Figure 1, it shows a schematic of a flotation cell with the various sub-processes. Typically, the particle-bubble attachment is considered to occur mostly in the turbulent region, near the impeller where high energy dissipation rates are often observed. CFD simulations have demonstrated that turbulence dissipation rate is one of the deterministic factors for bubble particle collisions (Koh, Manickam & Schwarz,2000; Liu & Schwarz,2009); experiments showed that the slip velocity of 2-10mm bubbles, a size very common in flotation cells, was influenced by turbulence intensity, and attachment rate could be computed from a model incorporating turbulence intensity (Evans *et al.*,2008). Also, detachment of particles and bubbles has been shown to be greatly affected by turbulence, too (King,1982). Detachment occurs when bubble particle composites are subjected to accelerations such that the detachment forces (including gravity) exceed surface tension forces. These phenomena depend partly on the size of the particles, but largely on the motion of particles and bubbles in the fluid flow, which is in the end determined by the strength of the velocity fluctuation, a property related to the turbulence intensity. Despite extensive research into turbulence in flotation, the effect of turbulence on flotation micro-processes remains less quantified and poorly understood from a quantitative viewpoint (Phan *et al.*,2003; Evans, Nguyen & Ata,2007). Turbulence also significantly affects the recovery of solids by entrainment (Schubert,1999), which is the micro-process whereby solid particles from the pulp zone are carried into the froth zone, then transported upwards and over the lip of the flotation cell. The

suspension is superior, for instance, in the highly turbulent conditions of the rotor zone but poorer in the upper quiescent zone. Entrainment is governed by the degree of suspension of particles just below the pulp froth interface and, therefore, the quiescent conditions in this upper zone help to reduce entrainment recovery.

Figure 1: A schematic of a flotation cell with the various sub-processes

Although turbulence plays a key role in wide range of industries, until now it has not been possible to undertake detailed model validation and sufficient study to turbulence due to the lack of proper measurement tools (Meng *et al.*,2014a; Meng, Xie, Runge, *et al.*,2015a), especially for multi-phase flows such as in flotation cells.

3. Experimental Quantifications of Turbulence

3.1 Variables used for characterising turbulence

Based on the above discussions, it is clear that an understanding of turbulence is very important to many industrial processes, such as mixing or flotation. Theoretical analysis of turbulence can be used to establish such an understanding; computer simulation can be employed to obtain a numerical result; but to validate these results, measurement of turbulence is necessary. The quantities that can be used to characterise turbulence include (Mathieu & Scott,2000):

- Root mean square velocity, usually represented by the standard deviation of a set of random velocity fluctuations.
- Pressure, *p*, a significant fluctuating quantity of turbulent flows.
- Turbulent kinetic energy, TKE, which is the root mean square of the fluid velocity fluctuation in all directions: TKE $= \left(V_1^{'2} + V_2^{'2} + V_3^{'2}\right)/2$.

The fluctuating velocity is usually characterised by measuring its standard deviation; the same goes with the fluctuating pressure. This property can be used to calculate turbulence kinetic energy. According to Mathieu and Scott(2000), TKE has long been considered an important quantity representing turbulence intensity, and it has been linked to flotation performance by a number of researchers (Li *et al.*,2010; Massey, Harris & Deglon,2012; Amini *et al.*,2013). By using one or several of these quantities, turbulence can be characterised.

Table 1. A summary on the turbulence quantification techniques.

3.2 Turbulence quantification techniques

To quantify turbulence in fluid flows, measurement tools are needed. There are quite many techniques that can be used to measure turbulence. Most of them do not directly measure velocity fluctuation or turbulent kinetic energy. Instead, they convert the quantities they measure to velocity fluctuation or turbulent kinetic energy through some transformation or calculation. Based on the physical quantities they measure, they can be categorized into the following groups.

- Pressure measurement techniques
- Optical techniques
- Electrical quantities measurement techniques
- Thermal quantities measurement techniques
- Tracing techniques.

A brief review of each group of techniques is provided in the following. The methods and technologies they use to quantify turbulence are discussed. Table 1 shows a summary on the experimental techniques reviewed in this paper.

3.2.1 Pressure measurement techniques

Piezoelectric sensor is based on converting measured pressure into turbulence related quantities. This section mainly outlines its principles and applications of turbulence quantification.

A piezoelectric sensor makes use of the piezoelectric effect to convert mechanical deformation to an electrical signal. It measures fluctuating pressure and can produce results of velocity, acceleration, strain or force. The piezoelectric effect is a natural property of certain substances. In Figure 2, it shows the geometry of plate-like piezoelectric specimen when the piezoelectric layer is sandwiched between top and bottom electrodes (Cao, et al. 2012). When deformed by an attracting or opposing force, charges of different polarities gather on the surface of the substance and can be detected by a voltage measurement device.

Figure 2: Piezoelectric effect (Cao, et al. 2012)

In turbulent flows, the fluid exhibits fluctuations in both velocities and kinetic energies. A piezoelectric sensor placed into a turbulent fluid deflects backwards and forwards and produces an alternative voltage. If the sensor is based on the pressure measurement, the measured fluctuating voltage signals would be proportional to fluid velocity fluctuation as indicated by Bakker et al. (2009). They employed eight Omega PX26-001DV piezoelectric pressure transducers to measure voltage signals caused by turbulence and vortex shedding in the tangential direction opposite to the impeller rotational direction in a 100l pilot scale Bateman flotation cell. From the measured standard deviation of the velocity, a cavern boundary was determined to distinguish the yielded turbulent fluid and the stagnant fluid around the impeller at various impeller speeds and was found to be generally agreed with CFD simulation results, as depicted in Figure 3 (points are measured boundary, crosses are CFD simulated boundary).

Figure 3: Piezoelectric pressure transducer measured caverns vs. CFD simulated ones at different impeller speed as per Bakker eta al. (2009).

The fluctuating voltage signal caused by pressure can also be converted to kinetic energy fluctuation, as demonstrated by Meng *et al.*(2014a). They used a MEAS LDT0-028K piezoelectric vibration sensor to measure the fluctuating drag force in the turbulent flow of a water only 60L flotation cell, which was proportional to the kinetic energy fluctuation. The measurements were taken along a vertical and a horizontal axis under different impeller speeds. The results were validated against LDA measurement results in the same flotation cell, as depicted in Figure 4.

From their findings, Meng *et al.*(2014b) also indicated that the kinetic energy fluctuation should be proportional to turbulent kinetic energy(TKE) in the fluid. Therefore, the piezoelectric vibration sensor measurement results can be used to interpret TKE in the liquid. They tested PVS in a Metso 300m^3 RCS industrial flotation cell, showing that the turbulence profile measured by the sensor varied with hydrodynamic conditions in an expected way.

The spatial scale of the piezoelectric vibration sensor is 1cm, which means only turbulence scale above this size can be measured; while the frequency response of the sensor can reach 10^9 Hz, which is sufficient to analyse any turbulent flow.

In their subsequent research, Meng *et al.* (2015b) applied the piezoelectric vibration sensor in two 3m^3 flotation cells to measure turbulence distribution and established mathematical models to predict turbulence distribution from flotation cell operational parameters. The models can predict turbulence zone volumes with rather a good accuracy. This work has demonstrated that the piezoelectric sensor is a good tool for quantifying turbulence.

(a) Comparison of vertical axis results.

(b) Comparison of horizontal axis results.

Figure 4: Comparison of piezoelectric sensor measured fluid drag force and LDA measured kinetic energy fluctuation as per Meng *et al.* (2014a). Different symbol shapes represent different impeller speeds, in which diamonds, squares and triangles correspond to 370, 450 and 550rpm, respectively.

3.2.2 Optical techniques

Modern optical techniques for studying turbulent flows in mineral processing include Laser Doppler Anemometry, and Particle Image Velocimetry.

3.2.2.1 Laser Doppler Anemometry

Laser Doppler Anemometry (LDA), also called Laser Doppler Velocimetry, utilises the Doppler shift in a laser beam to calculate velocity in a transparent or semi-transparent fluid seeded with tracing particles. In the early 1960s, the helium-neon laser was developed, which is monochromatic, collimated and coherent (Keating, 1988). These properties make helium-neon laser ideal for researching fluid flow properties when scattered by entrained particles in a fluid.

The principle of a LDA system is depicted in Figure 5. When entrained particles pass through the fringes, laser light is reflected and then collected and focused on a photo-detector by receiving optics. The fluctuating frequency represents the magnitude of the particle velocity and its direction on the plane created by the two laser beams. As the LDA is a non-intrusive measurement tool that can make multi-component bi-directional measurements with high temporal and spatial resolution, it is widely used to study the mean and turbulent characteristics of fluid flows. Since its spatial resolution is determined by the dimension of the two crossed laser beams, a typically resolvable scale would be 100μm in diameter and 1mm in length. With the development of modern data processing software, the temporal resolution of LDA is mainly restricted by the concentration of the seeding particles rather than the optics and the software. In a typical commercial use, a frequency range of 1KHz~10KHz can be achieved, which is sufficient to recover the frequency content of many flows (Jensen,2004).

Figure 5: A schematic of the LDA (Nie, *et al.*, 2013)

In an application to measure mean and turbulent gas bubble velocities in a stirred vessel, Morud and Hjertager(1996) employed a LDA device to measure the turbulent gas velocity in the radial, axial and tangential directions at various height, gas flow rates, and impeller speeds. The accuracy of the measurements was claimed to be within 1% of the actual value.The measured axial turbulent gas velocity at height 0.47D (D is the diameter of the vessel) and 4 different gas flow rates (0.49, 0.75, 1.0 and 1.33 vvm - volume gas per volume liquid per minute) are depicted in Figure 6.

Figure 6: Measured axial turbulent gas velocity at height 0.47D for different gas flow rates and impeller speeds as per Morud and Hjertager (1996).

The LDA measurement in single liquid phase in the Outokumpu flotation cells has been used to valid a CFD model (Tiitinen, et al., 2003). In another application, Kysela et al. (2013) measured the root mean square of the turbulent velocity 15mm under the impeller, from the impeller axis to the wall, in a stirred vessel and analysed the velocity power spectra. The measurements were taken under three different impeller speeds, and the results are depicted in Figure 7. The RMS turbulent velocity results were normalized to the impeller peripheral speed. The velocity PSDs were obviously dependent on the impeller speed, and it can be observed that they follow the trend of the Kolmogorov 5/3 law fairly good.

(a) RMS velocity (b) PSD of the velocity obtained at R =0.20

Figure 7: RMS and PSD of turbulent velocity measured in a stirred vessel by LDA as per Kyselaa et al. (2013).

In summary, the LDA is a powerful optical tool to quantify turbulence in fluid flows. With significant advancements in optical methods such as fibres, as well as advanced signal processing techniques and software development, the spatial and temporal resolution of LDA have been improved substantially to allow the higher accuracy of turbulence quantification. However, since it is an optical technique, its applications are mainly limited to one or two phase flows.

3.2.2.2 Particle Image Velocimetry

Particle Image Velocimetry (PIV) is an optical technique often used for flow visualisation and characterisation. Similar to LDA, it is a non-intrusive optical approach which utilises seeding particles to measure the velocity amplitude and direction of fluid flow across a 2D measurement plane. As far as particle concentration is concerned, PIV requires that individual particles can be identified in a single image but not necessarily tracked between images, which can be achieved with a medium concentration of seeding particles. When the seeding concentration is sufficiently low that individual tracking of particles is possible, the method is referred to as Particle Tracking Velocimetry.

Figure 8 below shows a typical PIV system (Johnson, et al., 2014). A PIV device consists of a CCD digital camera, a laser or a strobe designed to illuminate only the area to be photographed, an external trigger to manage the operation of the laser and exposure of the camera, the fluid, and the seeding particles.

Figure 8: A schematic of a PIV system (Johnson, et al., 2014)

As an example of application, Brady et al.(2006) employed a Digital Particle Image Velocimeter (DPIV), with CMOS digital camera and Copper vapour pulsing laser, that can record with great accuracy and kHz temporal resolution, velocity vectors of all three phases, namely the fluid, the solid particles and the air bubbles, in homogeneous isotropic turbulence generated by cylindrical grids. Figure 9 shows two sample images just above the turbulence grid and the resulting velocity field produced by cross correlation.

Figure 9: Two sample images with 80μm solid particles and flow tracers (top row), and 1.2 mm bubbles and flow tracers (bottom row) separated by 0.001 s and corresponding velocity field from cross correlation as per Brady et al. (2006).

Baldi, Hann and Yianneskis (2002) employed a PIV system comprising a PCO Sensicam SVGA camera with Nikon 55mm lenses and a 3WArgon laser generating a light sheet with a fibre optic and cylindrical lens fibre module. The system was used to analyse the entire flow field in a stirred vessel as well as small areas in the discharge stream region below the impeller. The mean flow velocity and rms velocity were measured and compared with LDA measurement results found in Fentiman *et al.*(1998), as depicted in Figure 10. In the figure, T is a dimension of the vessel, r is the radial distance from the centre of the vessel, V_{tip} is the impeller tip speed in m/s, and $\overline{U_z}$ and u_z' are mean and rms velocity, respectively.

Figure 10: a) Comparison of $\overline{U_z}/V_{tip}$ values in the plane z/T = 0.28 obtained by Fentiman *et al*. (1998) and PIV; b) Comparison of u_z'/V_{tip} values in the plane z/T = 0.18 obtained by Fentiman *et al.* (1998) and PIV.

It can be seen from the figure that the PIV measurement data agree well with LDA measurement data, proving the reliability of the PIV system being used.

PIV has been applied in a single-phase Wemco flotation cell and shown good agreement with CFD modelling (Kuang, et al., 2015). Both the PIV measurements and CFD modelling revealed two strong vortices, one below the rotor level and the other extending from the rotor region to the free surface. They also agreed well on a third small vortex in the region near the bottom of the disperser and outside the draft tube.

In summary, PIV is a powerful tool to quantify turbulence in fluid flows, with the ability to image the velocity field at high temporal and spatial resolution. With the advancement of the modern camera, laser and software technologies, PIV will be more and more widely used in areas requiring accurate measurement of turbulence quantities. The limitation of the PIV technique is that it depends on seeding particles to function, and the fluid being studied need to be transparent in general.

3.2.3 Electrical techniques

3.2.3.1 Conductivity measurement

In multiphase flows, conductivity varies at a point of measurement because of fluctuation in the proportion of a phase and the fact that there is a difference in conductivity between the phases. Therefore, conductivity measurement can be used to study phase concentrations or interactions between phases in the turbulent flows. When the suitable design of the probe and data processing techniques are used, the conductivity probe can also be used to quantify turbulence.

Chanson and Carosi (2007) presented their work based on conductivity probe measurement to analyse turbulence intensity level in an open channel air-water turbulent stream flows on a stepped chute conducted in a large-size facility with flow Reynolds numbers ranging from 3.8 E+5 to 7.1 E+5. They

employed a duo-tip conductivity probe (depicted in Figure 11) to obtain the temporal sequence of conductivity value at each tip. Because the big difference between the conductivity of air and water, the sequence obtained was in the form of a series of a square wave with varying duty cycle (determined by the size of the bubble pierced by the probe). The two temporal sequence were auto and cross-correlated to find the time averaged interfacial velocity and turbulence level. The time averaged interfacial velocity was given by V=Δx/T, where Δx is the distance between the two probe tips and T is the air-water interfacial travel time for which the cross-correlation function is maximum. The turbulent level was calculated by $T_u = 0.851 * \frac{\sqrt{\tau_{0.5}^2 - T_{0.5}^2}}{T}$, where $\tau_{0.5}$ is the time scale for which the cross-correlation function is half of its maximum value such as: $R_{xy}(T+\tau_{0.5}) = 0.5*R_{xy}(T)$, R_{xy} is the normalised cross-correlation function, and $T_{0.5}$ is the characteristic time for which the normalised auto-correlation function equals : $R_{xx}(T_{0.5}) = 0.5$.

Figure 11: Duo-tip conductivity probe and the deduced auto and cross correlation function (after Chanson and Carosi (2007)).

The measured time averaged interfacial velocity and turbulence intensity are presented in Figure 12. In the figure, $d_c = \sqrt[3]{Q_w^2/(gW^2)}$, where Q_w is water discharge rate (m^3/s), W is channel width (m); $V_c = \sqrt{gd_c}$, h is vertical step height of the chute. The variable y is distance (m) measured normal to the invert (or channel bed). The measurement was taken at step 10. Clearly can be seen in this figure is a turbulence profile varying with different y/d_c values. The correlation analysis also yielded a characterisation of the large eddies advecting the bubbles, with the turbulent length scales (the size of large vortical structures advecting air bubbles in the skimming flows) being $L_{xy}/Y_{90} \approx 0.05$ to 0.2 and turbulent time scales were within $0.01 \leqslant T\sqrt{g/Y_{90}} \leqslant 0.06$, where Y_{90} is characteristic depth (m) where the void fraction is 90%.

The results obtained in this work are significant as they have demonstrated the applicability of conductivity probe in a turbulent flow when specific probe design and the relevant algorithm is adapted to process the data obtained.

Figure 12: Time averaged interfacial velocity and turbulence level (after Chanson and Carosi (2007)).

3.2.3.2 Electrical resistance tomography

ERT gained its first acceptance in the 1920s as a geophysical technique for detecting underground structures by converting the electrical measurement data gathered from the surface or from electrodes in boreholes to images. Arrays of electrodes were inserted into the ground. Currents were applied to one pair of electrodes and voltage responses at all others were measured to acquire an image of the underground structure, thereby making it possible to get a more accurate profile of, for instance, oil shales (Dickin & Wang,1996). This technique was further refined by Dines and Lytle (Dines & Lytle,1979; Lytle & Dines,1980), who combined conventional electrical probing measurement with the more recent tomographic process. ERT has been successfully applied to measure solid/liquid and gas/liquid mixing in hydrocyclones, flotation columns, packed columns, liquid-liquid extraction, precipitation processes and hydraulic conveying. In theory, any process where the primary continuous phase is to some extent electrically conductive while other elements have different values of resistivity can be investigated and monitored by ERT.

An ERT system consists of three main components: the electrode sensors, the data acquisition (DAQ) system and the data inversion/image reconstruction software. Fixed at equal distances around the vessel being measured, the electrodes inject current into the fluid and measure the voltage response to enable reconstruction of the variation in resistance across the plane/planes of interest. The purpose of the DAQ system is to do the analogue to digital conversion required to enable communication to and from the data processing computer and the electrodes. The most commonly used real-time reconstruction algorithm uses a regularized and iterative Newton-Raphson algorithm (Hua & Woo,1990) to calculate the conductivity vector describing the measurement plane.

When air bubbles move through the ERT measurement plane, the conductivity distribution fluctuates with turbulence. By measuring these fluctuations, turbulence information can be extracted. Meng *et al.*

(2014b and 2015a) fabricated an intrusive ERT probe sized approximately 4cm in diameter and used the probe in a 60L flotation cell with air and water. The cell was operated at different air flow rate and impeller speeds while they measured the voltage fluctuation and analysed the voltage measurement data through a Green-Kubo method, which linearly correlates the electrical flux to an applied force in the measurement field through a transport coefficient. The transport coefficient can be calculated from the autocorrelation coefficients of the measured voltage values. The applied force, on the other hand, can be correlated with velocity fluctuation through the momentum theory. Therefore, the velocity fluctuation was correlated with the electrical flux through the transport coefficient. The measurement results were compared with kinetic energy fluctuation measurement results obtained with a piezoelectric vibration sensor, the results for air rate 40L/min is depicted in Figure 13. Similar results can be obtained for air rate 80 and 100L/min. It can be seen that there is a squared correlation between the ERT and the piezoelectric sensor's results, which validates that the ERT-derived quantity is some measure of velocity fluctuation.

Figure 13: Velocity fluctuation at air rate 40L/min measured by ERT and a comparison with PVS results as per Meng et al. (2015).

Though the ERT has been validated as capable of measuring velocity fluctuation, the temporal and spatial resolutions are quite limited. The ERT device used by Meng *et al.* (2015a) has a maximum data frame rate of 1 kHz, meaning that the frequency response is limited to this frame rate. The current derived velocity fluctuation, on the other hand, is just an average value on the measurement plane defined by the electrode array. Therefore, the spatial resolution is on the scale of several cm, which is insufficient to distinguish smaller turbulence eddies in most scenarios. However, the ERT data can be analysed with a finite element method, and the spatial resolution can possibly be reduced to the size of an element. Also, the beauty of the ERT measurement tool is that it can work in multiphase flows. Therefore, there exists incentives to develop further the ERT as a turbulence measurement tool from both application and algorithm research level.

3.2.4 Thermal techniques

Thermal measurement techniques usually employ a hot wire heated with a supplied current/voltage to measure mean and rms velocities in turbulent flows. As the fluid flows over the wire, the convective heat transfer to the fluid cools the wire. Therefore, this technique is also called hot wire anemometer. There are two subtypes of the hot wire anemometer; one is the constant current anemometer (CCA), for which the current is maintained at a constant value and the change in wire resistance due to the change in velocity results in changing voltage across the wire. In constant temperature operation (CTA), the current to the wire is adjusted to maintain a constant temperature of the wire and the resulting voltage across the wire is again a manifestation of the velocity. Either a CCA anemometer or a CTA anemometer can be chosen for measuring rms turbulence intensities ranging from 0.1% to 10% of the local mean velocity. If the turbulence intensity is less than 0.1%, then CCA is a better choice because it has a super low noise amplifier or a transformer coupled input. However, if turbulence intensity is more than 10%, then a constant temperature anemometer (CTA) should be used as it is a linearized anemometer (Bradshaw & Woods,1971).

A typical CTA measurement setup is depicted in Figure 14. The setup consists of a probe attached to a probe support and probe cable, a Wheatstone bridge, servo, and signal conditioner which serve as the anemometer, and an A/D converter plugged into a computer for processing signals.

Figure 14: Typical CTA measurement system (Jorgensen, 2002).

An example of CTA application in agitated vessels was reported by Amini et al.(2013) who employed a CTA in both a 5 L and a 60 L flotation cell to measure the local velocity and velocity fluctuation, based on which averaged turbulent kinetic energy (TKE) was correlated with impeller speed. By assuming that TKE does not change with the addition of air or solids, Sauter mean bubble size d32 under different impeller speeds was correlated with TKE at different air flow rates.

The beauty of the hot wire anemometry technique is that fine scale velocity fluctuations at high frequencies can be detected via very fine wire sensors and electronics with servo-loop techniques. Since the output of the hot wire sensor is analogue voltage with very high temporal resolution with very little information loss during sampling, it is suitable for analysing spectra. The spatial resolution of the hot wire probe is determined by the length of the wire lw. The smallest scale reported by Bailey

et al.(2010) was 50 microns. Further down-scale of such wire was impossible because the ratio of lw to the wire diameter d needs to be large enough so as to suppress the end-conduction effect, which attenuates the measured turbulence fluctuations and leads to undesirable errors in the data(Hultmark, Ashok & Smits,2011). The temporal response of a typical 5 microns diameter hot wire was reported to be 1.3ms by Bailey et al.(2010). However, the nano-scale probe sized 100 nm×2μm×60μm reported by them can achieve a temporal response as short as 50μs. Test of such a nano-scale probe in a grid turbulence and comparison with traditional CTA and CCA probes have shown that the measurement results agreed well and that the nano-scale probe can be used to measure micro-turbulence inflows with Reynolds number as high as 1.2×10^6. It was also envisaged that well-resolved measurements can be made inflows with Reynolds numbers up to 3.6×10^6 when the size of the sensing wire can be reduced to 100 nm×100 nm×20μm. The weak point of a hot wire probe is that it is susceptible to environmental factors such as temperature change and solid contamination. Therefore, its use is mainly limited to air flow or one phase liquid flows.

3.2.5 Particle Tracking Velocimetry

Particle Tracking Velocimetry (PTV) is a modern technique in that seeding particles are tracked to reveal their Lagrangian trajectory in the fluid flow. There are two different experimental methods for PTV, namely the two-dimensional PTV and the three-dimensional PTV. The 2D PTV measures a 2D slice of the flow illuminated by a laser sheet by recording the images of low-density seeding particles and tracks each particle for several frames. In 3D PTV, multiple cameras are used to record images in an illuminated 3D volume to track the flow tracers by using photogrammetry (Dore, et al., 2009).

An example of the application of a 3D PTV was presented by Kasagi and Matsunaga (1995). They made detailed flow measurements in a turbulent channel flow using a 3D particle tracking velocimeter and calculated various turbulent statistics from numerous instantaneous vector distributions. Results were found to agree well with DNS (Direct Numerical Simulation) results obtained by Le et al. (1993), as depicted in Figure 15.

Figure 15: Comparison of 3D PTV measured flow properties (dots) with DNS obtained results (lines) (after Kasagi and Matsunaga (1995)). (a) mean velocity; (b) streamwise rms turbulent fluctuation; (c) Reynolds shear stress.

An attempt has been made to use a submersible imaging system in in situ measurements of industrial flotation cells, which shows potential for measuring undisturbed fluid velocity field (Honkanen, et al. 2010). A 3D PTV is capable of quantifying turbulence in transparent turbulent flows, but it is not applicable in opaque flows.

Positron Emission Particle Tracking (PEPT) is another kind of 3D particle tracking technique developed in recent years. Initially developed for medical imaging purposes, it was first adopted in engineering at the University of Birmingham. The basic principle of PEPT is based on positron annihilation. A single ("tracer") particle is labelled with a radionuclide that decays via beta-plus decay, generating two gamma photons, each of which has an energy of 511 keV, moving in precisely opposite directions. An array of detectors (a PET "camera") is used to detect the two gamma rays simultaneously, which defines the line along which the annihilation occurred. Detection of a few such events in a very short time interval allows the position of the tracer particle to be triangulated in three dimensions. Location in space of the tracer particle may be achieved at a frequency of up to 250 Hz with an accuracy which depends on the speed and activity of the tracer particle. Many of the reported work to apply PEPT in turbulent flows deal with velocity measurement. The quality of the measurement for flotation processes is related to the spatial and temporal precision of the PET scanner and the characteristics of the tracer (Cole, et al., 2014). Their results showed that tracer particles require sufficient activity for accurate tracking. Guida et al.(2009) employed PEPT to study the mixing of a concentrated suspension of coarse glass particles and liquid in a vessel stirred by a pitched blade turbine, visualizing the Lagrangian trajectory of a single positron-emitting particle, which was then used to obtain the detailed Eulerian path of the two-phase flow inside the vessel. Pianko-Oprych et al. (2009) compared the velocity measurements made by PEPT with those made using PIV of water in the same vessel and found excellent agreement. Excellent velocity measurement results were also obtained for solid suspensions with concentrations as high as 5wt%, which was not achievable using PIV. Chiti et al.(2011) used PEPT to study the turbulent flow in a baffled vessel agitated by a Rushton turbine. The Lagrangian velocity obtained from the PEPT was converted to an Eulerian velocity that was then

compared with LDA measurement results in the literature. The excellent agreement between the two results validated that the PEPT technique could be used to obtain accurate velocity data in the vessel.

The PEPT is capable of revealing particle trajectories in opaque turbulent flows in very small scale vessel. However, it is very challenging to apply the PEPT to measure velocity fluctuation as the mass of water surrounding the tracer absorbs a portion of the γ-rays, decreasing the signal to noise ratio (Chiti, et al., 2011). Therefore, is not able to quantify turbulence.

4. Conclusions

Turbulence plays an important role in many industries, and it needs to be better understood. However, turbulence flow has the feature of irregular motion at different time scales and spatial scales. It is critical to find appropriate quantification technique for turbulence in the system of interest to acquire useful information and data for the system.

This paper provides a review of turbulence quantification techniques that can be applied to fluid flows, outlining their system structure, principles of measurement, the range of application as well as the advantages and disadvantages associated with using the techniques in various applications. A summary on the techniques reviewed in this paper is shown in Table 1. The optical techniques, LDA and PIV can achieve high spatial and temporal resolution, but their applications are limited to transparent flows and only work well in one or two phase flows. With specific design, they can be used to quantify turbulence fluctuations. However, generally, they only work well in a one phase fluid as the presence of particles or air bubbles block and interfere with the measurement. Hotwire probes have high spatial and temporal resolutions in turbulence quantification due to their fine size and analogue signal, but they are susceptible to environmental factors such as contamination. They work well in the air, or one phase fluid flows, but may not be able to work in multiphase flows. Conductivity probe, Electrical Resistance Tomography (ERT) and Piezoelectric Sensor are techniques that can quantify turbulence in multiphase flows, but their spatial resolutions are limited. For ERT, there is a possibility to improve the spatial resolution by employing an element analysis based on finite element method (FEM). Particle Tracking Velocimetry (PTV) can reveal particle trajectories in multiphase flows; it can also measure turbulence related parameters such as velocity fluctuation and Reynolds stress. Positron Emission Particle Tracking (PEPT) cannot be used to quantify turbulence although it can be used to determine the Lagrangian trajectory of particles.

This review provides an insight into what has been used historically for measurement but also highlights several techniques such as Piezoelectric Sensor, ERT and Conductivity probe that have the potential to be used to study fluid properties for three-phase flows in industries. Further development of those techniques for obtaining turbulence information in multiphase flows will assist engineers in equipment design and operation optimisation and control. The quantitative measurement can also provide data for validation of CFD simulations.

References

Amini, E., Bradshaw, D. J., Finch, J. A.& Brennan, M. (2013) Influence of turbulence kinetic energy on bubble size in different scale flotation cells. *Minerals Engineering, 45*, 146-160.

Avila, K., Moxey, D., de Lozar, A., Avila, M., Barkley, D.& Hof, B. (2011) The Onset of Turbulence in Pipe Flow. *Science, 333*, 192-196.

Bailey, S. C. C., Kunkel, G. J., Hultmark, M., Vallikivi, M., Hill, J. P., Meyer, K. A., . . . Smits, A. J. (2010) Turbulence measurements using a nanoscale thermal anemometry probe. *J. Fluid Mech., 663*, 160-179.

Bakker, C. W., Meyer, C. J.& Deglon, D. A. (2009) Numerical modelling of non-Newtonian slurry in a mechanical flotation cell. *Minerals Engineering, 22*(11), 944-950.

Baldi, S., Hann, D.& Yianneskis, M. (2002, 8-11 July， 2002) *On the measurement of turbulence energy dissipation in stirred vessels with PIV techniques*, Proc. 11th International Symposium on Applied Laser Techniques in Fluid Mechanic. Lisbon.

Batchelor, G. K. (1967) (Book)An Introduction to Fluid Dynamics. Published by Cambridge University Press.

Bradshaw, P.& Woods, W. A. (1971) (Book)An Introduction to Turbulence and its Measurement--A volume in Thermodynamics and Fluid Mechanics Series. Published by Elsevier Ltd.

Brady, M. R., Telionis, D. P., Vlachos, P. P.& Yoon, R.-H. (2006) Evaluation of multiphase flotation models in grid turbulence via Particle Image Velocimetry. *International Journal of Mineral Processing, 80*(2–4), 133-143.

Cao, Z., Zhang, J. & Kuwano, H. (2012) Design and characterization of miniature piezoelectric generators with low resonant frequency. *Sensors and Actuators A* 179, 178– 184

Chanson, H.& Carosi, G. (2007) Turbulent time and length scale measurements in high-velocity open channel flows *Experiments in Fluids, 42*(3), 385-401.

Chiti, F., Bakalis, S., Bujalski, W., Barigou, M., Eaglesham, A.& Nienow, A. W. (2011) Using positron emission particle tracking (PEPT) to study the turbulent flow in a baffled vessel agitated by a Rushton turbine: Improving data treatment and validation. *Chemical Engineering Research and Design, 89*(10), 1947-1960.

Cole K., Buffler A., Cilliers J.J., Govender I., Heng J.Y.Y., Liu C., Parker D.J., Shah U.V., van Heerden M., Fan X. (2014), A surface coating method to modify tracers for positron emission particle tracking (PEPT) measurements of froth flotation, *Powder Technology*, 263, 26-30.

Cutter, L. A. (1966) Flow and turbulence in a stirred tank. *A.1.Ch.E. Journal, 12*(1), 35-45.

Dickin, F.& Wang, M. (1996) Electrical resistance tomography for process applications. *Meas. Sci. Technol., 7*, 247-260.

Dines, K. A.& Lytle, R. J. (1979) Computerized geophysical tomography. *Proceedings IEEE, 67*(7), 1065-1073.

Dore, V., Moroni, M. & Menach, M.L. (2009) Investigation of penetrative convection in stratified fluids through 3D-PTV. *Exp Fluids*, 47, 811-825.

Eames, I.& Flor, J. B. (2011) New developments in understanding interfacial processes in turbulent flows. *Phil. Trans. R. Soc. , A*(369), 702-705.

Jameson, G. J., Nguyen, A. V.& Ata, S. (2007). The flotation of fine and coarse particles. In M. C. Fuerstenau, G. J. Jameson & R.-H. Yoon (Eds.), *Froth Flotation: A Century of Innovation* (pp. 329-351). Denver, CO, USA: SME.

Evans, G. M., Doroodchi, E., Lane, G. L., Koh, P. T. L.& Schwarz, M. P. (2008) Mixing and gas dispersion in mineral flotation cells. *Chemical Engineering Research and Design, 86*(12), 1350-1362.

Fallenius, K. (1987) Turbulence in flotation cells. *International Journal of Mineral Processing, 21*(1–2), 1-23.

Fentiman, N. J., Hill, N. S., Lee, K. C., Paul, G. R.& Yianneskis, M. (1998) A novel profiled blade impeller for homogenization of miscible liquids in stirred vessels. *Transactions of the Institution of Chemical Engineers, 76*(Part A), 835-842.

Guida, A., Fan, X., Parker, D. J., Nienow, A. W.& Barigou, M. (2009) Positron emission particle tracking in a mechanically agitated solid–liquid suspension of coarse particles. *Chemical Engineering Research and Design, 87*(4), 421-429.

Holman, J. P. (2002) (Book)Heat Transfer.Edited by B. Stenquist. Published by McGraw Hill.

Honkanen, M., Eloranta, H. & Saarenrinne, P. (2010) Digital imaging measurement of dense multiphase flows in industrial processes. *Flow Measurement and Instrumentation* 21, 25-32

Hua, P.& Woo, J. (1990). Electrical Impedance Tomography. In A. Hilger (Ed.), *Electrical Impedance Tomography*. Bristol U.K.: J.G. Webster.

Hultmark, M., Ashok, A.& Smits, A. J. (2011) A new criterion for end-conduction effects in hot-wire anemometry. *Meas. Sci. Technol. , 22*(055401).

Jensen, K. D. (2004) Flow Measurements. *J. Braz. Soc. Mech. Sci., 26*(4), 400-419.

Johnson, B., Tian, W., Zhang, K. & Hu, H. (2014) An experimental study of density ratio effects on the film cooling injection from discrete holes by using PIV and PSP techniques. *International Journal of Heat and Mass Transfer*, 76, 337–349

Jorgensen, F. E. (2002) (Book)How to measure turbulence with hot-wire anemometers-a practical guide. Published by DANTEC Dynamics A/S.

Kasagi, N.& Matsunaga, A. (1995) Three-dimensional particle-tracking velocimetry measurement of turbulence statistics and energy budget in a backward-facing step flow. *International Journal of Heat and Fluid Flow, 16*(6), 477-485.

Keating, M.P., (1988) Geometric physical and visual optics. Published by Elsevier Health Sciences.

King, R. P. (1982) (Book)Principles of Flotation, (Vol. 3).Published by South African Institute of Mining and Metallurgy.

Koh, P. T. L., Manickam, M.& Schwarz, M. P. (2000) CDF simulation of bubble-particle collisions in mineral flotation cells. *Minerals Engineering, 13*(14–15), 1455-1463.

Kolmgorov, A.N., (1941), The local structure of turbulence in incompressible viscous fluid for very large Reynolds numbers. First published in Russian inDokl. Akad. Nauk SSSR (1941) 30(4). This translation by V. Levin, reprinted here with emendations by the editors of this volume. *Proc. R. Soc. Lond*. A (1991) 434, 9-13.

Kysela, B., Konfršt, J.& Chara, Z. (2013) LDA measurements and turbulence spectral analysis in an agitated vessel. *EPJ Web of Conferences, 45*, 01055-p.01051-p.01056.

Laín, S., Bröder, D., Sommerfeld, M.& Göz, M. F. (2002) Modelling hydrodynamics and turbulence in a bubble column using the Euler–Lagrange procedure. *International Journal of Multiphase Flow 28*, 1381-1407.

Le, H., Moin, P.& Kim, J. (1993) *Direct numerical simulation of turbulent flow over a backward-facing step.*, Proc. 9th symposium on turbulent shear flows. Kyoto, Japan. 13.12.11-13.12.16.

Li, L., Liu, J., Wang, L.& Yu, H. (2010) Numerical simulation of a self-absorbing microbubble generator for a cyclonic-static microbubble flotation column. *Mining Science and Technology (China), 20*(1), 88-92.

Liu, T. Y.& Schwarz, M. P. (2009) CFD-based multiscale modelling of bubble–particle collision efficiency in a turbulent flotation cell. *Chemical Engineering Science, 64*(24), 5287-5301.

Lytle, R. J.& Dines, K. A. (1980) Iterative ray tracing between boreholes for underground image reconstruction. *IEEE Transactions on Geoscience and Remote sensing, 18*, 234-240.

Massey, W. T., Harris, M. C.& Deglon, D. A. (2012) The effect of energy input on the flotation of quartz in an oscillating grid flotation cell. *Minerals Engineering, 36–38*(0), 145-151.

Mathieu, J.& Scott, J. (2000) (Book)An introduction to turbulent flow. Published by Cambridge University Press.

Meng, J., Xie, W., Brennan, M., Runge, K.& Bradshaw, D. (2014a) Measuring turbulence in a flotation cell using the piezoelectric sensor. *Minerals Engineering, 66-68*, 84-93.

Meng, J., Xie, W., Brennan, M., Tabosa, E., Runge, K.& Bradshaw, D. (2014b) *New techniques for measuring turbulence in flotation cells*, Proc. XXVII International Mineral Processing Congress Santiago Chile. 70-81.

Meng, J., Xie, W., Runge, K.& Bradshaw, D. (2015a) Measuring Turbulence in a Flotation Cell using Electrical Resistance Tomography. *Meas. Sci. Technol., 26*(11), 1-12.

Meng, J., Xie, W., Tabosa, E., Runge, K.& Bradshaw, D. (2015b) *Turbulence modelling for flotation cells based on piezoelectric sensor measurement data*, Proc. 7th International Flotation Conference. Cape Town,SA.

Morud, K. E.& Hjertager, B. H. (1996) LDA measurements and CFD modelling of gas-liquid flow in a stirred vessel. *Chemical Engineering Science, 51*(2), 233-249.

Nguyen, A. V.& Schulze, H. J. (2004). Colloidal science of flotation, M. Dekker, New York, 840 pp.

Nie, X, Zhou, J. & Long, X. (2013). Estimation of the velocity and acceleration for the laser Doppler signal. *Optik*, 124, 2829-2832.

Phan, C. M., Nguyen, A. V., Miller, J. D., Evans, G. M.& Jameson, G. J. (2003) Investigations of bubble-particle interactions. *Int. J. Miner. Process., 72*, 239-254.

Pianko-Oprych, P., Nienow, A. W.& Barigou, M. (2009) Positron emission particle tracking (PEPT) compared to particle image velocimetry (PIV) for studying the flow generated by a pitched-blade turbine in single phase and multi-phase systems. *Chemical Engineering Science, 64*(23), 4955-4968.

Rao, M. A.& Brodkey, R. S. (1972) Continuous flow stirred tank turbulence parameters in the impeller stream. *Chemical Engineering Science, 27*, 137-156.

Sanyal, J., Vasquez, S., Roy, S.& Dudukovic, M. P. (1999) Numerical simulation of gas–liquid dynamics in cylindrical bubble column reactors. *Chem. Eng. Sci., 54*, 5071-5083.

Schubert, H. (1999) On the turbulence-controlled microprocesses in flotation machines. *International Journal of Mineral Processing, 56*(1–4), 257-276.

Streeter, V. L. (1966) Fluid mechanics (4th Ed). Published by McGraw-Hill Book Company.

Tabor, M. (1989) Chaos and Integrability in Nonlinear Dynamics: An Introduction. Published by Wiley-Interscience.

Tiitinen, J., Vaarno, J. & Grönstrand, S. (2003) Numberical modeling of an outokumpu flotation device. *Third International Conference on CFD in the Minerals and Process Industries*, CSIRO, Melbourne, Australia. 10-12 December 2003. 167-170.

Wilcox, C. D. (1998) Turbulence Modeling for CFD, (2nd Edition). Published by DCW Industries.

Wu, J., Nguyen, B., Lane, G., Wang, S., Parthasarathy, R.& Graham, L. J. (2012) Process Intensification in Stirred Tanks. *Chem. Eng. Technol, 35*(7), 1125-1132.

Figures and Tables:

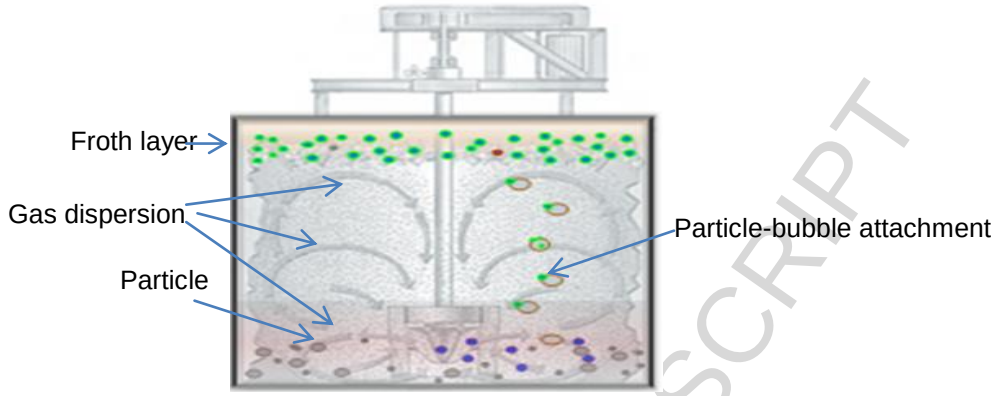

Figure 1: A schematic of a flotation cell with the various sub-processes

Table 1. A summary on the turbulence quantification techniques.

Techniques	Phases of fluids	Response	Parameters	Application in flotation	Main references
PVS	3	Sensor deformation	Mechanical forces	Lab and Industry	Cao, et al., 2012; Bakker et al., 2009; Tabosa et al., 2012, Meng et al., 2014a, 2014b and 2015b.
LDA	2	Laser	Velocities	Lab	Morud & Hjertager, 1996; Tiitinen, et al., 2003; Kyselaa et al., 2013.
PIV	1	Laser	Velocities	Lab	Baldi, et al., 2002; Brady et al., 2009; Fentiman et al., 1998; Kuang, et al., 2015
Conductivity sensor	3	Conductivity	Electrical field	Lab	Chanson and Carosi, 2007
ERT	3	Conductivity	Electrical field	Lab	Hua & Woo,1990; Dickin & Wang,1996; Meng et al., 2014b and 2015a
CTA	2	Heat/cooling	Thermal field	Lab	Bradshaw & Woods,1971; Bailey et al., 2010; Hultmark, et al.,2011; Amini et al., 2013
PTV	2	Laser	Velocities	Lab and Industry	Le et al. 1993; Kasagi and Matsunaga 1995; Dore, et al., 2009; Honkanen, et al. 2010
PEPT	3	Gamma photons	Positron annihilation	Lab	Guida et al., 2009; Pianko-Oprych et al. , 2009; Chiti et al.,2011; Cole, et al., 2014

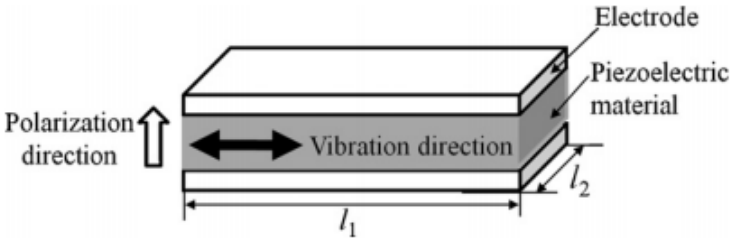

Figure 2: Piezoelectric effect (Cao, et al. 2012)

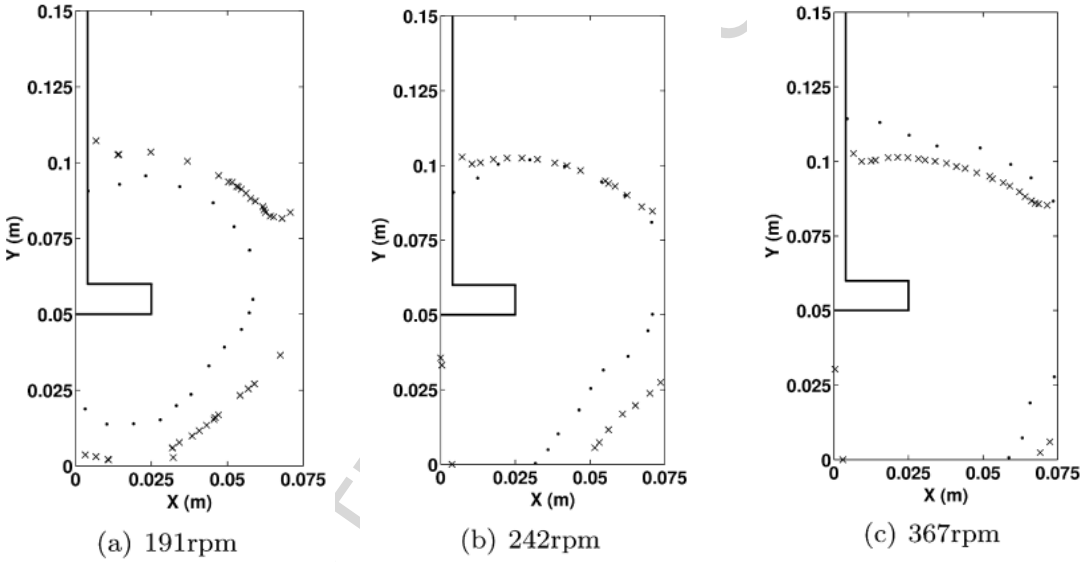

Figure 3: Piezoelectric pressure transducer measured caverns vs. CFD simulated ones at different impeller speed as per Bakker eta al. (2009).

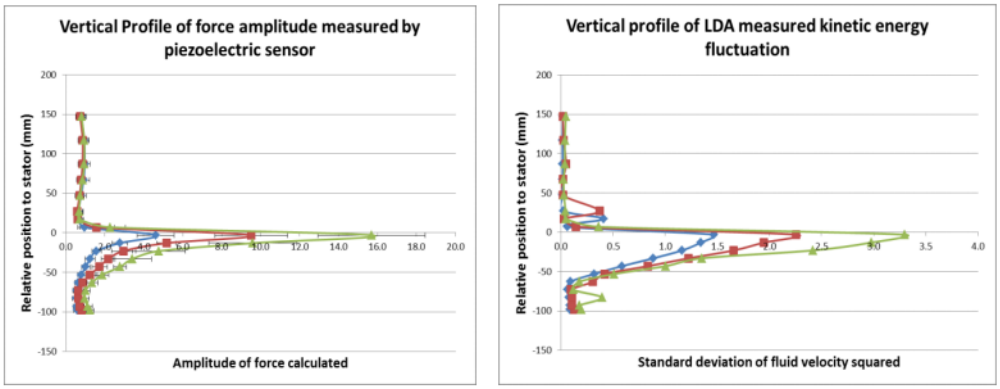

(c) Comparison of vertical axis results.

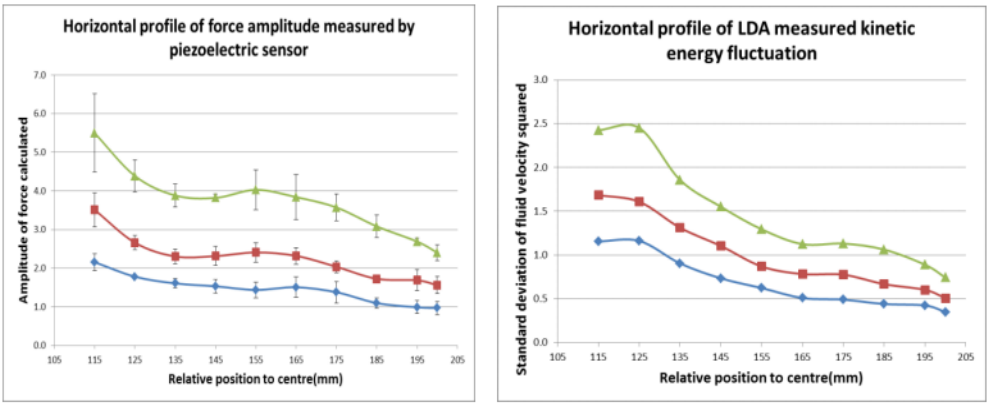

(d) Comparison of horizontal axis results.

Figure 4: Comparison of piezoelectric sensor measured fluid drag force and LDA measured kinetic energy fluctuation as per Meng *et al.* (2014a). Different symbol shapes represent different impeller speeds, in which diamonds, squares and triangles correspond to 370, 450 and 550rpm, respectively.

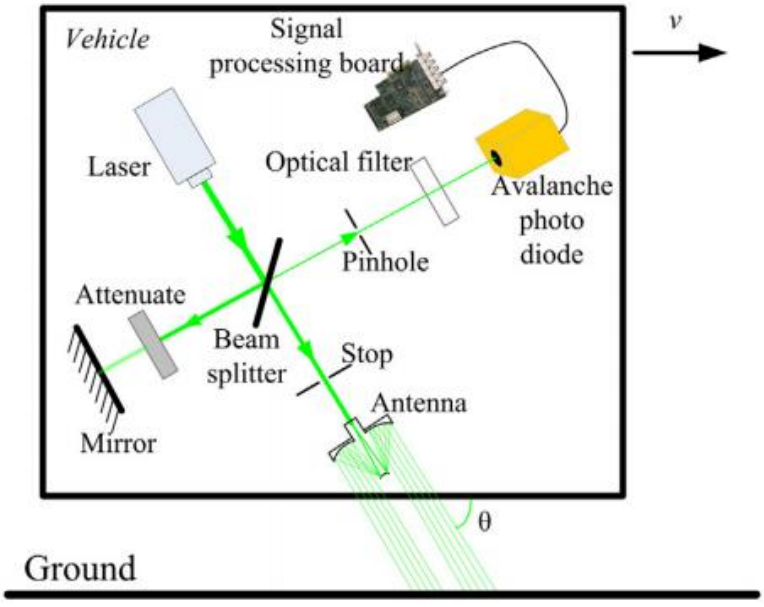

Figure 5: A schematic of the LDA (Nie, *et al.*, 2013)

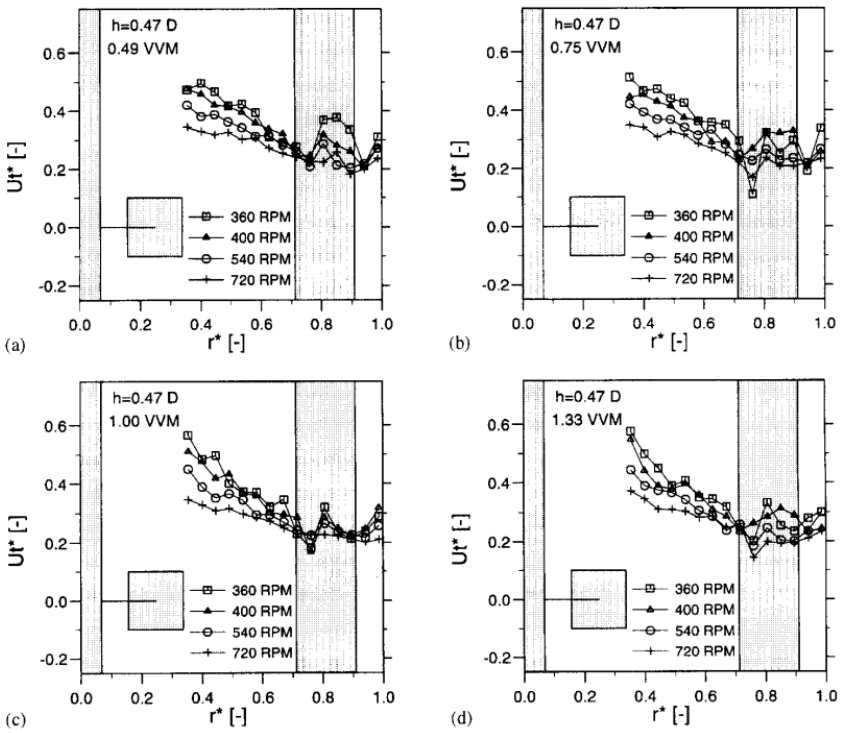

Figure 6: Measured axial turbulent gas velocity at height 0.47D for different gas flow rates and impeller speeds as per Morud and Hjertager (1996).

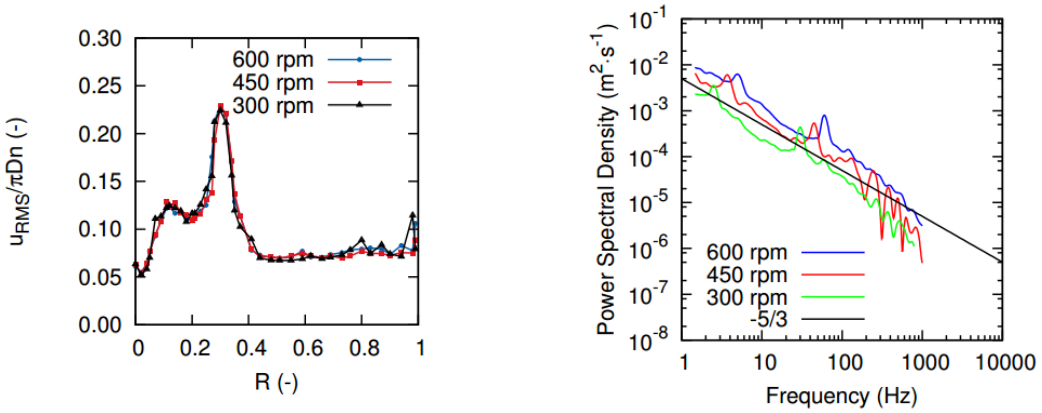

(c) RMS velocity (d) PSD of the velocity obtained at R =0.20

Figure 7: RMS and PSD of turbulent velocity measured in a stirred vessel by LDA as per Kyselaa et al. (2013).

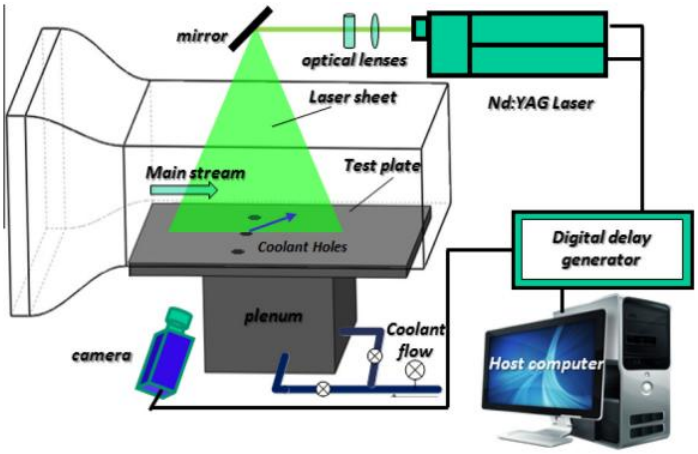

Figure 8: A schematic of a PIV system (Johnson, et al., 2014)

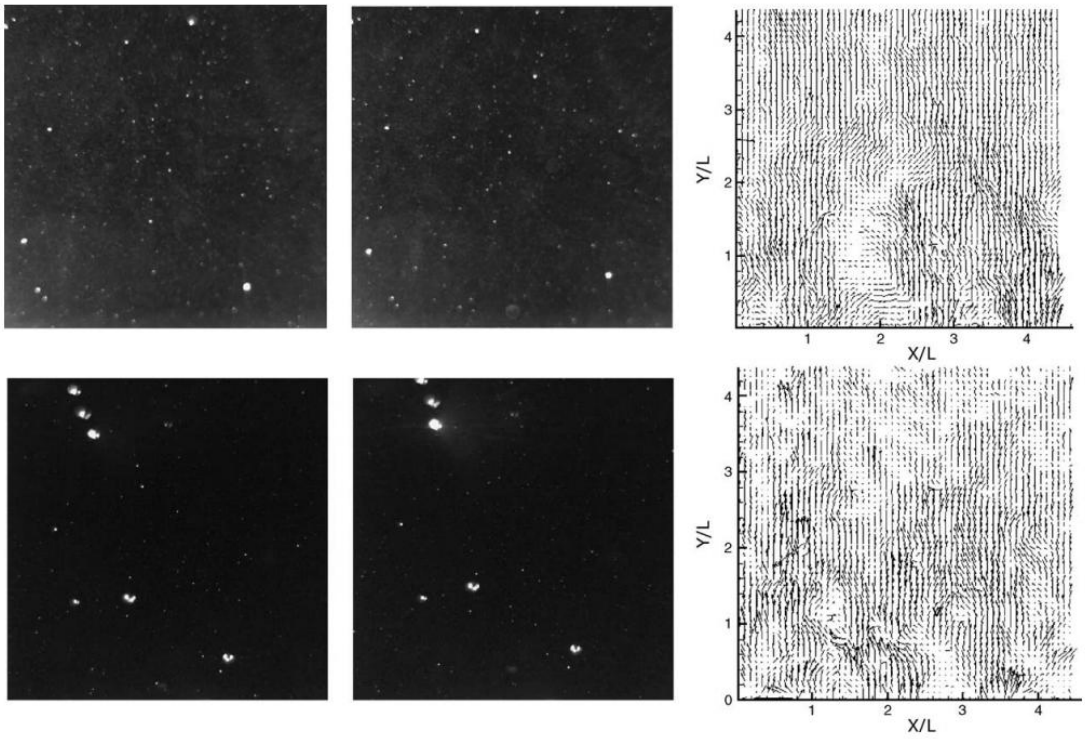

Figure 9: Two sample images with 80μm solid particles and flow tracers (top row), and 1.2 mm bubbles and flow tracers (bottom row) separated by 0.001 s and corresponding velocity field from cross correlation as per Brady et al. (2006).

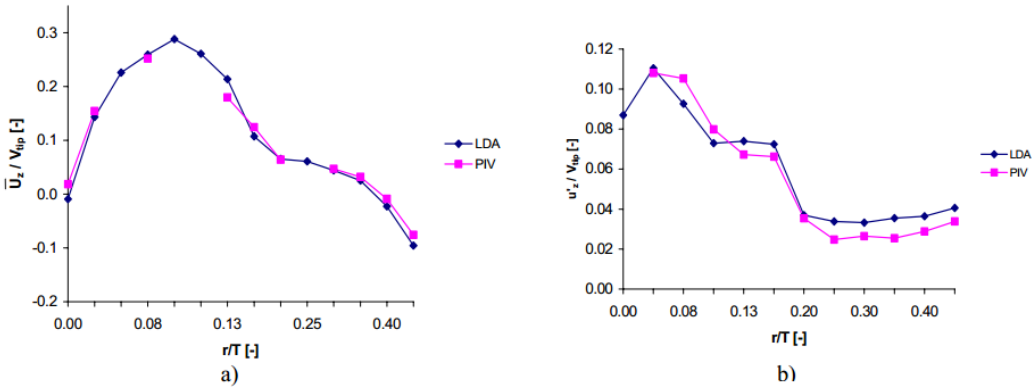

Figure 10: a) Comparison of $\overline{U_z}/V_{tip}$ values in the plane z/T = 0.28 obtained by Fentiman *et al.* (1998) and PIV; b) Comparison of $u_z^{'}/V_{tip}$ values in the plane z/T = 0.18 obtained by Fentiman *et al.* (1998) and PIV.

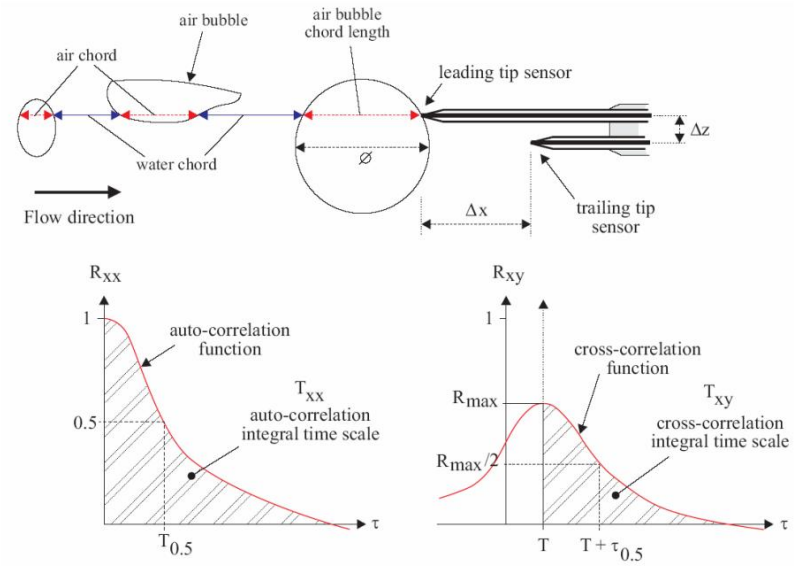

Figure 11: Duo-tip conductivity probe and the deduced auto and cross correlation function (after Chanson and Carosi (2007)).

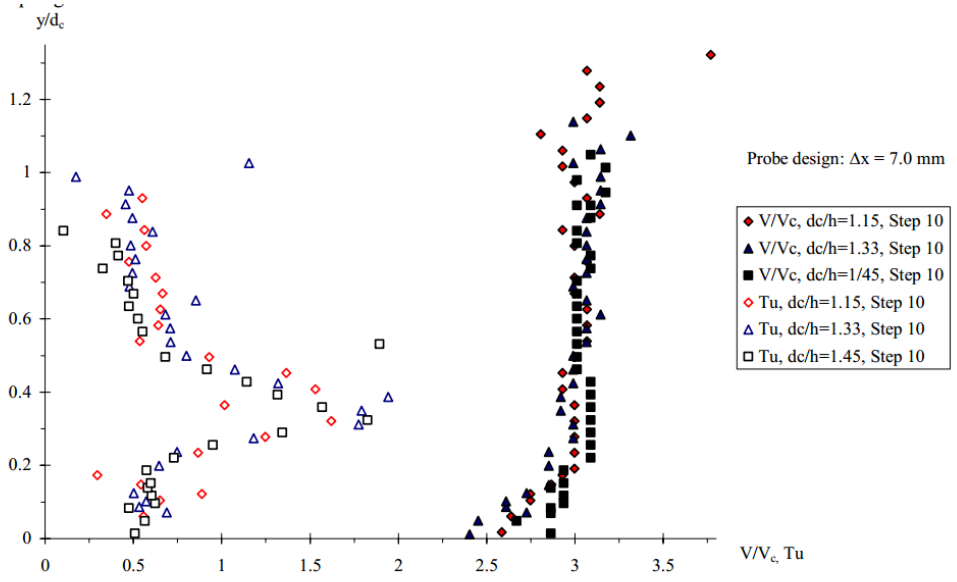

Figure 12: Time averaged interfacial velocity and turbulence level (after Chanson and Carosi (2007)).

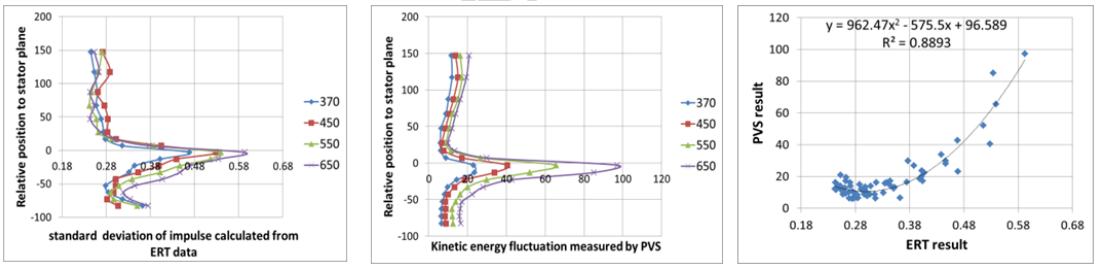

Figure 13: Velocity fluctuation at air rate 40L/min measured by ERT and a comparison with PVS results as per Meng et al. (2015).

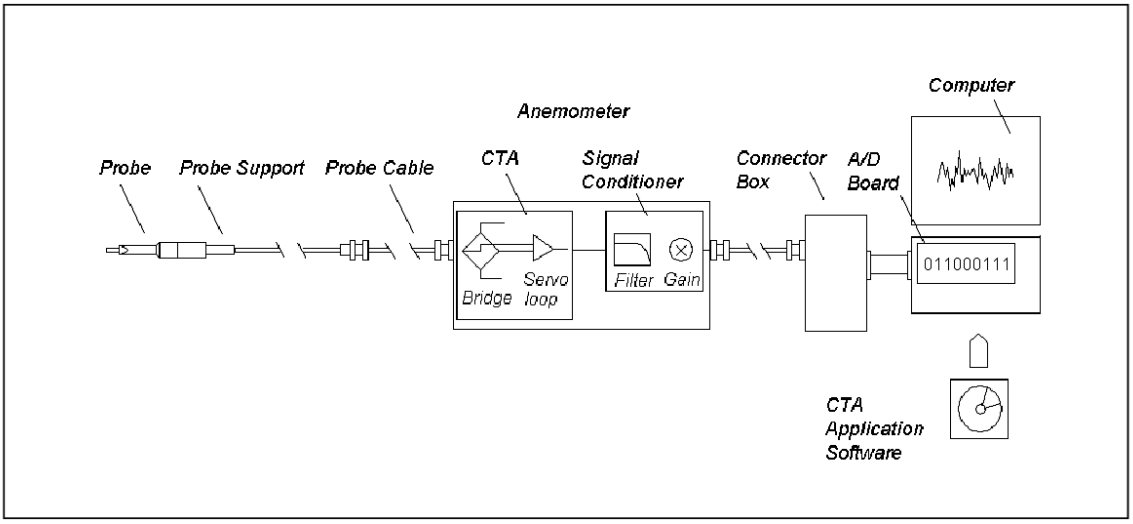

Figure 14: Typical CTA measurement system (Jorgensen, 2002).

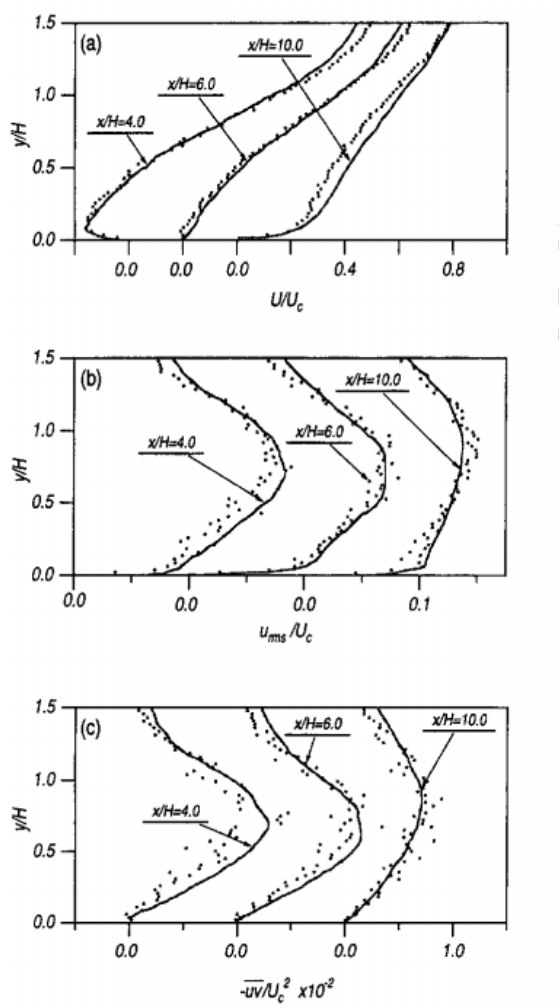

Figure 15: Comparison of 3D PTV measured flow properties (dots) with DNS obtained results (lines) (after Kasagi and Matsunaga (1995)). (a) mean velocity; (b) streamwise rms turbulent fluctuation; (c) Reynolds shear stress.

Highlights

- Different quantification techniques of turbulence in the literature have been reviewed.
- Many measurement techniques cannot be used to quantify turbulence in multiphase flows.
- Piezoelectric Sensor, Electrical Resistance Tomography and Conductivity Probe have the potential to be used to quantify turbulence for three-phase flotation pulps.